Analytical theory for extracellular electrical stimulation of nerve with focal electrodes

II. Passive myelinated axon

J. T. Rubinstein

Department of Otolaryngology, Cochlear Implant Research Laboratory, Eaton-Peabody Laboratory, Massachusetts Eye and Ear Infirmary, Boston, Massachusetts 02114 USA

ABSTRACT The cable model of a passive, myelinated fiber is derived using the theory of electromagnetic propagation in periodic structures. The cable may be excited by an intracellular source or by an arbitrary, time-varying, applied extracellular field. When the cable is stimulated by a distant source, its properties are qualitatively similar to an unmyelinated fiber. Under these conditions relative threshold is proportional to the cube of the source distance and inversely proportional to the square of the fiber diameter. Electrical parameters of the model are chosen where possible, from mammalian peripheral nerve and anatomic parameters from cat auditory nerve. Several anatomic representations of the paranodal region are analyzed for their effects on the length and time constants of the fibers. Sensitivity of the model to parameter changes is studied. The linear model reliably predicts the effects of fiber size and electrode-fiber separation on threshold of cat dorsal column fibers to extracellular electrical stimulation.

INTRODUCTION

There have been many attempts to model electrotonus in myelinated nerve analytically. Most studies treat the node as a lumped parameter with a distributed parameter internode (18, 24, 26, 30, 34, 35, 43, 44). Koide was the first to consider a completely distributed node–internode unit, but his analysis was limited to the DC case (23). Dun performed the first AC analysis for the distributed node–internode, making predictions of nodal anatomy (15). Although an error in his logic was reported by FitzHugh (18), Dun's technique for calculating the complex attenuation constant of the node–internode unit was correct. A similar approach, taking advantage of the near periodicity of myelinated fibers, will be used in this study.

In previous papers (41, 42), the history of models for extracellular electrical stimulation of nerve has been reviewed and a technique described for applying cable models of unmyelinated fiber to the problem of extracellular stimulation. Since then, models for stimulation of fiber bundles have been reported using a bidomain model to account for current flow in both intracellular and interstitial compartments (2, 36). Others have considered the effects of the statistical distribution of fiber size, position, and nodal location (46). Rattay has demonstrated the importance of the "activating function," the second spatial derivative of the stimulus field (39). Andrietti and Bernardini have illustrated that an "equivalent" uniform representation of the myelinated fiber is a useful approximation of the segmented model (4). Colombo and Parkins have used a spatially extended modification of the McNeal model (27, 40) to explain the long chronaxies associated with electrical stimulation of the auditory nerve (14, 33). This model included an excitable unmyelinated terminal on the peripheral dendrite of the spiral ganglion cell.

As McNeal pointed out, the weakest part of his model was the assumption that the myelin sheath is a perfect insulator (27). He had no means to analyze the error induced by this assumption but did not believe it should significantly affect the strength-duration curve. It will be demonstrated here that the effect of myelin conductance and capacitance significantly increases the time constant for extracellular stimulation of a passive cable. This result must also apply to nonlinear cables. Thus, any attempt to derive the chronaxie of a model auditory nerve fiber must account for the myelin resistance and capacitance, as was done in a recently reported model of cochlear implantation (16).

In this paper, model results will be compared with single unit recordings from electrically stimulated cat dorsal column fibers as described by BeMent and Ranck (7). Their results were modeled using a steady-state approach, and ignored current flow across the internodal membrane (8). It will be demonstrated that a cable model for electrical stimulation of myelinated fiber can account for the observed threshold changes due to changes in fiber size, electrode-fiber separation, and stimulus polarity.

MODEL AND ASSUMPTIONS

The model myelinated fiber and monopolar stimulating electrode are illustrated in Fig. 1. The physiological

0006-3495/91/09/538/18 $2.00

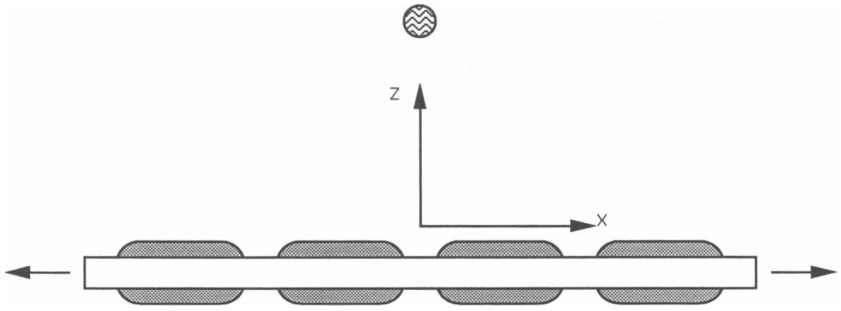

FIGURE 1 Myelinated fiber model in the field of a monopolar spherical current source. Fiber extends to + and $-\infty$ as indicated by the arrows.

assumptions are those of FitzHugh (17): (*a*) The fiber is represented by an equivalent circuit consisting of an axial resistance and membrane resistance and capacitance distributed in x. (*b*) One-dimensional longitudinal flow of intracellular current is present. (*c*) One-dimensional radial flow of membrane current is present. (*d*) The membrane properties of the axon may be represented by interspersed regions of nodal and internodal membrane impedance. (*e*) Nodes of Ranvier are periodically distributed in x.

In addition, the membrane is assumed to be purely passive, with no voltage sensitive conductances and with electrical properties comparable to those of a true fiber near the resting potential. The fiber is placed in a purely resistive, homogeneous, and isotropic medium. It is assumed that the presence of the fiber does not distort the applied extracellular field.

The symbols to be used are defined in Table 1. Model fiber parameters, chosen to represent an average sized peripheral process of a cat spiral ganglion cell at 37°C, are given in Table 2.

THEORY

In this section the equations describing electrotonus of a myelinated fiber will be derived. The results will permit the derivation of an expression describing the membrane potential of a passive myelinated fiber induced by any extracellular field. First a Green's function will be obtained for a uniform cable and for simple nonuniform cables. Floquet's theorem will be applied to determine the Green's function for a periodically nonuniform cable. Integration of this Green's function over the applied extracellular field gives the desired result: the membrane potential induced by that field.

The application of cable theory to the problem of extracellular electrical stimulation of uniform axons results in the following partial differential equation for the intracellular potential $V(x, t)$

$$-\lambda^2 V_{xx} + \tau V_t + V = \Psi + \tau \Psi_t, \tag{1}$$

where $\Psi(x, t)$ is the applied extracellular field and V_{xx} is the second spatial derivative of V in the x direction (39, 41). An alternative solution to this equation than that given in reference 41 is obtained by taking the Fourier

TABLE 1 Symbol definitions

Symbol	Definition	Units
a	Internodal axon radius	*mm*
c_1	Nodal membrane capacitance	*F/mm*
c_2	Internodal membrane capacitance	*F/mm*
C_1	Specific node capacitance	F/mm^2
d	Internodal axon diameter	*mm*
D	Internodal fiber diameter	*mm*
g	Axon/fiber diameter (d/D)	
I	Current through source electrode	*mA*
k	Spatial frequency	*radians/mm*
l	Unit fiber length ($2l_1 + l_2$)	*mm*
l_1	Half of node length	*mm*
l_2	Internodal length ($L * D$)	*mm*
L	Internodal length/fiber diameter	
λ_1	Nodal length constant	*mm*
λ_2	Internodal length constant	*mm*
$\Psi(x, z, t)$	Extracellular applied potential	*mV*
Q	Complex attenuation constant	mm^{-1}
ρ	Resistivity of medium	Ωmm
r_a	Axial resistance	Ω/mm
r_1	Nodal membrane resistance	Ωmm
r_2	Internodal membrane resistance	Ωmm
R_a	Axoplasm resistivity	Ωmm
R_1	Specific node resistance	Ωmm^2
t	Time	*ms*
τ_1	Nodal time constant	*ms*
τ_2	Internodal time constant	*ms*
$V(x, t)$	Intracellular potential	*mV*
$V_m(x, t)$	Membrane potential	*mV*
ω	Temporal frequency	*radians/ms*
x	Distance along fiber	*mm*
z	Distance from fiber	*mm*
Z	Input impedance	Ω

TABLE 2 **Model fiber parameters at 37°C**

Parameter	Value	Reference
d	1.5 μm	25
D	2.5 μm	
g	0.6	5
L	92	5, 25
$2l_1$	1 μm	9, 25
l_2	230 μm	
l	231 μm	
R_a	1,063 Ωmm	28
R_1	831 Ωmm^2	12, 13
C_1	0.041 $\mu F/mm^2$	12
r_2	209 $M\Omega mm$	45
c_2	1.6 pF/mm	45
λ_1	17.1 μm	
λ_2	589 μm	
τ_1	34.1 μs	
τ_2	334.4 μs	

Values without references are calculated from referenced values. In deriving specific membrane properties, node length is considered to be 1.5 μm for the large fibers used in the voltage-clamp studies (9).

transform of Eq. 1 with respect to t. This gives

$$\overline{V}_{xx} - Q^2\overline{V} = -Q^2\overline{\Psi},$$

where

$$Q = \frac{1}{\lambda}\sqrt{1 + j\omega\tau}. \tag{2}$$

The Green's function of the Fourier transform of V, $\overline{G}(x, \omega)$ is obtained by assigning $\Psi(x, t) = \delta(x)\delta(t)$

$$\overline{G} = E_+e^{-Qx} + E_-e^{Qx} \quad x > 0,$$

where the first term on the right is the positive-going signal and the second is the negative-going signal. Q is the complex attenuation constant. As the solution to the homogeneous or undriven equation is also an exponential, Q is identical to that derived for intracellular stimulation. Later it will be shown that Q is of great importance in describing the extracellular "polarizability" of a fiber.

Uniform axon

Consider an infinitely long, uniform axon with a spatial impulse located at $x = 0$. The Green's function of the frequency response, $\overline{G}(x, \omega)$ is given by

$$\overline{G}_{xx} - Q^2\overline{G} = -Q^2\delta(x).$$

The only physically possible solution is the decaying signal,

$$\overline{G}(x, \omega) = Ae^{-Q|x|},$$

where A is obtained by integrating the differential equation for the Green's function from 0− to 0+, yielding

$$\overline{G}(x, \omega) = \frac{Q}{2}e^{-Q|x|}. \tag{3}$$

Note that if spatial frequency is denoted by k, the Fourier transform in x of $\overline{G}$ is

$$\overline{\overline{G}} = \frac{Q^2}{Q^2 + k^2} \tag{4}$$

which is the spatial frequency response of the continuous axon as given in reference 41.

If the axon is placed in the field of a monopolar point source at $(x = 0, z)$ passing a current I, the Fourier transform of the intracellular potential is given by convolving the Green's function, given by Eq. 3, with the applied field $\Psi(x, z)$. This has a closed form solution at $x = 0$ which is given by

$$\overline{V}(z, \omega) = \frac{\rho IQ}{8\pi}\int_{-\infty}^{\infty}\frac{e^{-Q|x|}}{\sqrt{x^2 + z^2}}dx. \tag{5}$$

Manipulating Eq. 5, using (3.387) of reference 21 and subtracting the external field gives the transmembrane potential

$$\overline{V}_m(z, \omega) = \frac{\rho IQ}{8}[\boldsymbol{H}_0(Qz) - N_0(Qz)] - \frac{\rho I}{4\pi z}, \tag{6}$$

where $\boldsymbol{H}_0$ is the Struve and N_0 the Bessel function of the second kind of order zero.

The spatial Fourier transform of the intracellular potential at $x = x', x' \neq 0$, is obtained by multiplying the spatial frequency response of the axon given in Eq. 4 by the spatial Fourier transform of the applied field. Using (3.754) of reference 21 and the shifting rule for Fourier transforms gives the spatial frequency content for the applied field $\Psi(x - x')$ produced by a point current source at (x', z)

$$\frac{\rho I}{2\pi}K_0(|k||z|)e^{-jkx'}. \tag{7}$$

Thus, the intracellular potential is given by an inverse Fourier transform

$$\overline{V}(x, z, \omega) = \frac{\rho I}{4\pi^2}\int_{-\infty}^{\infty}\frac{Q^2}{Q^2 + k^2}K_0(|k||z|)e^{jk(x-x')}dk. \tag{8}$$

Note that at $x = x'$ this reduces to an integral found in (6.566) of reference 21 which returns the closed form given in Eq. 6.

Nonuniform axon

Consider a nonuniform axon composed of multiple segments i each of length l_i. Each segment may have different properties but the properties do not vary within a segment. Properties for segment i are denoted with a subscript i. For the case of zero extracellular potential, the intracellular potential is given by Eq. 1 in each segment. Thus, the longitudinal current and intracellular potential for the ith segment may be written

$$V_i(x) = V_i(0)\cosh Q_i x - I_i(0)\frac{r_a}{Q_i}\sinh Q_i x \quad 0 \le x \le l_i \quad (9)$$

$$I_i(x) = -\frac{Q_i}{r_a}V_i(0)\sinh Q_i x + I_i(0)\cosh Q_i x \quad 0 \le x \le l_i, \quad (10)$$

where $x = 0$ is at the beginning of the segment, r_a is the axial resistance per unit length, and Q_i is the complex attenuation constant for that particular segment as given by Eq. 2. These may be arranged to form a matrix equation relating the input and output of the segment

$$\begin{bmatrix} V_i(0) \\ I_i(0) \end{bmatrix} = \begin{bmatrix} A_i & B_i \\ C_i & D_i \end{bmatrix} \begin{bmatrix} V_i(l_i) \\ I_i(l_i) \end{bmatrix}.$$

Simple manipulation yields

$$A_i = \cosh Q_i l_i$$

$$B_i = \frac{r_a}{Q_i}\sinh Q_i l_i$$

$$C_i = \frac{Q_i}{r_a}\sinh Q_i l_i$$

$$D_i = A_i.$$

If several segments are linked together, the input and output are related by the product of the transmission matrices for each segment. For a three-segment cable where the third segment is identical to the first, the matrix coefficients are given by

$$A = A_1^2A_2 + A_1B_1C_2 + A_1B_2C_1 + A_2B_1C_1$$

$$B = 2A_1A_2B_1 + B_1^2C_2 + A_1^2B_2$$

$$C = 2A_1A_2C_1 + A_1^2C_2 + B_2C_1^2$$

$$D = A.$$

Periodically nonuniform axon

Consider the node–internode unit, illustrated in Fig. 2. Apply the results of the previous section to the case of an infinitely long, myelinated fiber, exicted by an extracellular spatial potential impulse or by an intracellular point source. Because each node–internode unit is exactly like any other, the membrane potential at any point will be identical to the membrane potential one unit away,

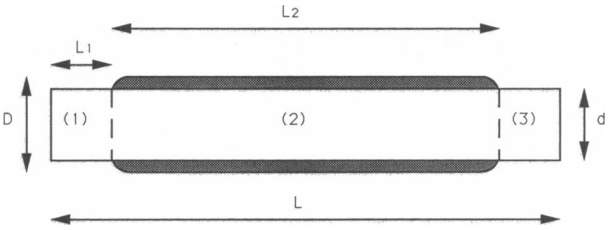

FIGURE 2 The node-internode unit.

decreased in amplitude and increased in phase. Thus although the field changes nonuniformly within a unit, it decays uniformly from unit to unit, or

$$V(x + l) = V(x)e^{-Ql}$$

$$I(x + l) = I(x)e^{-Ql},$$

where Q is the attenuation constant for the node–internode unit and l is the length of the unit, $2l_1 + l_2$. This represents the application of Floquet's theorem to a periodic cable (47). Note that this uniform unit to unit decay holds only if the extracellular potential is zero. This is the case for a fiber in an infinite medium with an intracellular source or with extracellular stimulation *by a spatial impulse.*

Letting $\eta = e^{Ql}$ and defining the intracellular potential and longitudinal current at the end of the node–internode unit as V_e and I_e, respectively, we see that

$$\begin{bmatrix} A & B \\ C & D \end{bmatrix} \begin{bmatrix} V_e \\ I_e \end{bmatrix} = \eta \begin{bmatrix} V_e \\ I_e \end{bmatrix}$$

which requires that the determinant

$$\begin{vmatrix} A - \eta & B \\ C & D - \eta \end{vmatrix} = 0.$$

Considering only the positive going, or decaying wave, the solution of the resulting quadratic yields

$$Q = \frac{1}{l}\cosh^{-1} A. \quad (11)$$

It will be demonstrated that the Q given by Eq. 11 approximates a weighted average of the attenuation constants Q_i for each segment of the periodic cable.

Thus, if the voltage is specified at a point, say $V(0) = V_0$, it is known at all integral multiples of l through

$$V(nl) = V_0e^{-Qnl} \quad n = 0, 1, 2, \ldots$$

and within a segment through the use of Eqs. 9 and 10. A simple example of this is seen with intracellular stimulation. An intracellular electrode, passing a current I_0 is

placed at the center of a node at $x = 0$. The extracellular resistance is assumed negligible and the membrane parameters are defined in Table 2. V_0 can be determined from

$$\begin{bmatrix} V_0 \\ I_0 \end{bmatrix} = \begin{bmatrix} A & B \\ C & D \end{bmatrix} \begin{bmatrix} V_0 e^{-Ql} \\ I_0 e^{-Ql} \end{bmatrix}$$

which reduces to

$$V_0 = I_0 \frac{B}{e^{Ql} - A}$$

defining the input impedance Z. The exact solution for the membrane potential is then given by Eqs. 9 and 10. An approximate solution may be obtained by

$$V = I_0 Z e^{-Qx}. \tag{12}$$

These are both plotted in Fig. 3. Electrotonic decay in myelinated fibers appears piecewise-linear with changes in slope occuring at nodes of Ranvier. A detailed view of this slope change is given in Fig. 4. It shows the membrane potential in a node and its neighboring internode when the fiber is stimulated by an intracellular electrode one node away. Although electrotonic decay is exponential in uniform node or internode, there is an impedance mismatch at the node–internode junction when the two are combined. This mismatch results in approximately linear electrotonic decay along the internode. The slope of decay changes at nodes so that the node to node decay is globally exponential.

Far-field solution

The previous section indicates that the exact solution for the Green's function of a periodic cable is cumbersome. It is difficult to integrate the Green's function over a continuous applied field because the function is described by different equations in each segment. This theory, while complex, yields important results and is described in the appendix. For the special case of far-field solutions, it is possible to avoid complication provided the above exact Green's function can be approximated by the continuous function

$$\overline{G}(x) = \frac{Q}{2} e^{-Q|x|}. \tag{13}$$

Andrietti and Bernardini have performed a similar approximation for current flow in a myelinated fiber (4) but did not take advantage of periodicity. Eq. 13 is identical to Eq. 3 for a continuous cable but Q is obtained from Eq. 11 instead of Eq. 2. It equals the exact solution at the center of each node and as such represents spatial samples of the exact solution. In theory the approximation will be accurate if the sampling frequency exceeds the Nyquist rate. This will be the case if the applied field has no spatial frequency components greater than one-half the spatial sampling frequency, two pi times the reciprocal of the length l of the unit membrane. Fig. 5 illustrates the spatial frequency content of the approximate response of a model fiber to a monopolar point source at three distances, z. This

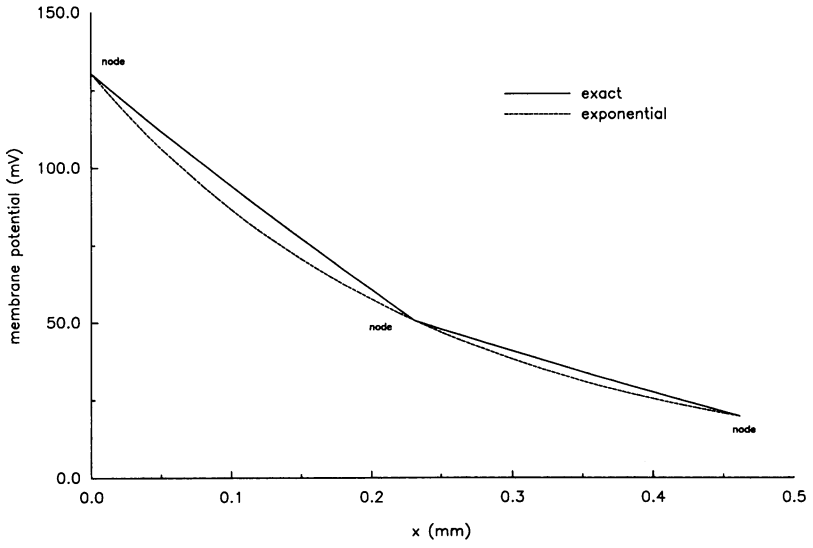

FIGURE 3 Membrane potential at first three nodes for intracellular stimulation at center of first node. Stimulus is 1 nA DC current. Fiber parameters from Table 2. Exact solution given by Eqs. 9 and 10. Exponential or approximate solution given by Eq. 12.

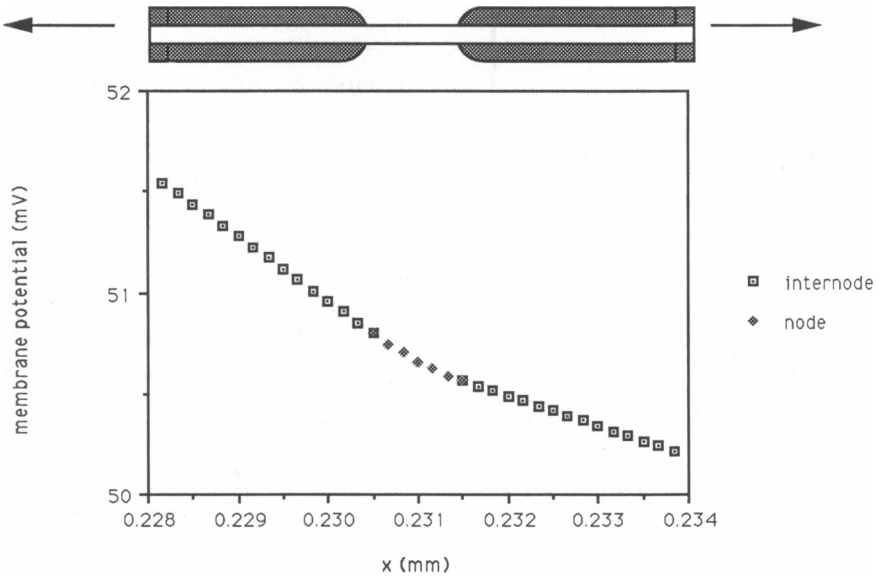

FIGURE 4 Detail of membrane potential in vicinity of the second node for the fiber model in Fig. 3.

response is calculated by multiplying the spatial frequency content of the source, Eq. 7 with $x' = 0$, by the spatial frequency response of the approximation, Eq. 4, for the DC case. The bulk of the energy for all three distances lies at spatial frequencies less than $k = 6.8$, one-fourth of the sampling frequency. Thus, for stimulating myelinated fibers where the length $l \leq 0.231$ mm and the distance $z \geq 1$ mm, the approximation given by Eq. 13 is not degraded by aliasing. The distance z beyond which this approximation becomes valid is smaller at higher temporal frequencies. Because the internodal distance $l_2 = l - 2l_1$, calculations such as those in Fig. 5 can define the fiber sizes and perpendicular distances z for which the far-field approximation applies.

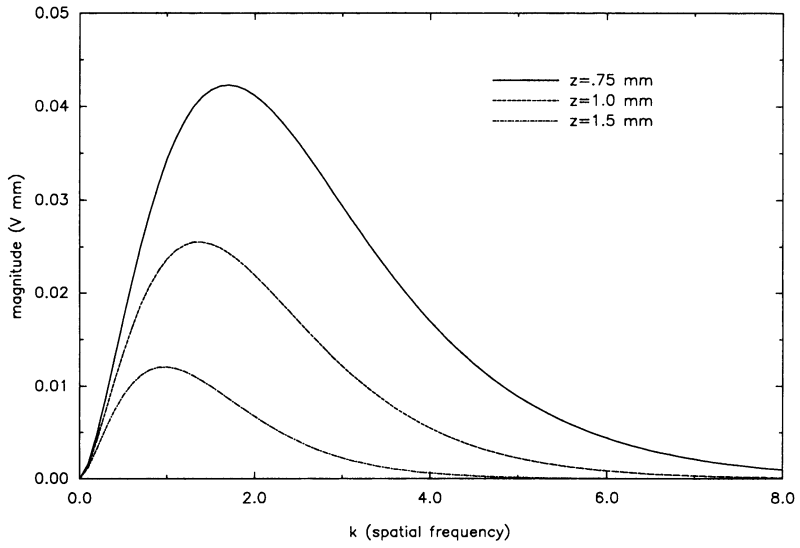

FIGURE 5 Spatial frequency content of far-field response to a monopolar point source at $z = 0.75$ mm, $z = 1$ mm, $z = 1.5$ mm. Model fiber parameters given in Table 2. Units of spatial frequency are radians per millimeter. Temporal frequency is DC and $\rho I = 2\pi$ V mm.

RESULTS

Membrane potential profiles

Consider an infinite myelinated cable with parameters defined in Table 2. Place it in a homogeneous, isotropic medium of resistivity ρ with a monopolar point source passing a current I at a distance z from the closest node of Ranvier. This node and the source are both positioned at $x = 0$ as illustrated in Fig. 1. As long as $z > 1$ mm, a distance chosen somewhat arbitrarily from Fig. 5 to represent a conservative value, the far-field approximation applies and the intracellular potential at the center of each node is given by Eq. 8 with Q given by Eq. 11. These two equations can be rapidly solved on a small computer and the membrane potential plotted for various stimulus frequencies and source distances.

Figs. 6 and 7 illustrate the effect of varying source distance and stimulation frequency on the spatial distribution of the passive membrane response. These figures are useful in the construction of nonlinear models, as they may help decide parameters such as the number of active nodes and the total fiber length needed to create an adequate numerical model for a given stimulation paradigm. The figures also illustrate that the distribution of membrane potential is affected differently by increases in distance and frequency. Although both decrease the response of the fiber model, increasing z increases the spread of membrane potential within a fiber, while increasing frequency decreases this spread.

The curves in Figs. 6 and 7 are qualitatively similar to those obtained for unmyelinated cables, as the equation from which they are obtained has the same form. The quantitative difference results from the use of a different attenuation constant Q. For a myelinated cable, Q approximates a weighted average of the attenuation constants of the node and of the internode. Another major difference is that these curves are only an accurate portrayal of the membrane potential at the nodes; they do not necessarily apply between nodes. Because fiber excitation only occurs at nodes, however, this is not a significant restriction.

Nearest node

At the center of the node nearest to the electrode, or $x = 0$, Eq. 8 reduces to Eq. 6. Because only the far-field case is being considered at present, a further simplification is possible. For large values of the argument Qz, Eq. 6 has an asymptotic expansion, given in reference 1, which rapidly converges. For $Qz \gg 1$, the first term of this expansion alone is sufficient to give an accurate estimate. Under these circumstances, and subtracting the extracellular potential, the membrane potential becomes

$$\overline{V}_m(z, \omega) = \frac{-\rho I}{4\pi Q^2 z^3}. \tag{14}$$

This simple expression defines the important geometric parameters of extracellular electrical stimulation. It demonstrates that the induced depolarization is propor-

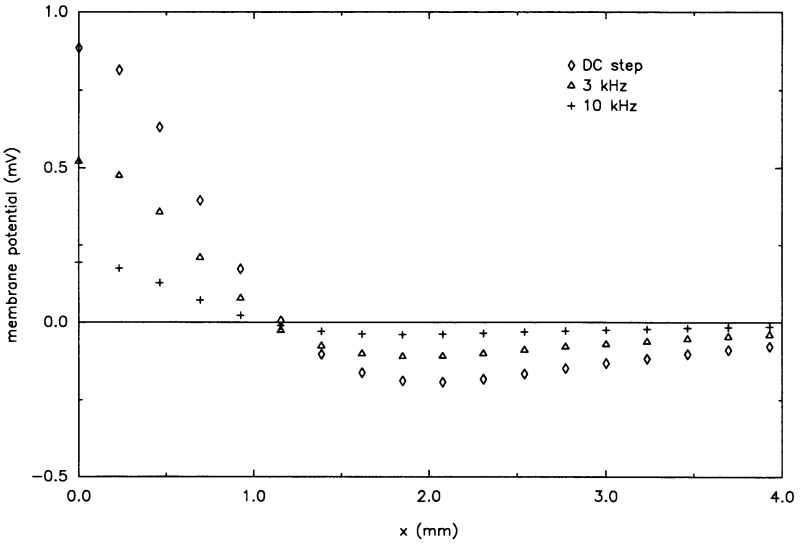

FIGURE 6 Profiles of the steady-state membrane potential for DC step, 3 and 10 kHz stimuli. Current is 1 mA at $z = 1.5$ mm. Results valid only at nodes of Ranvier.

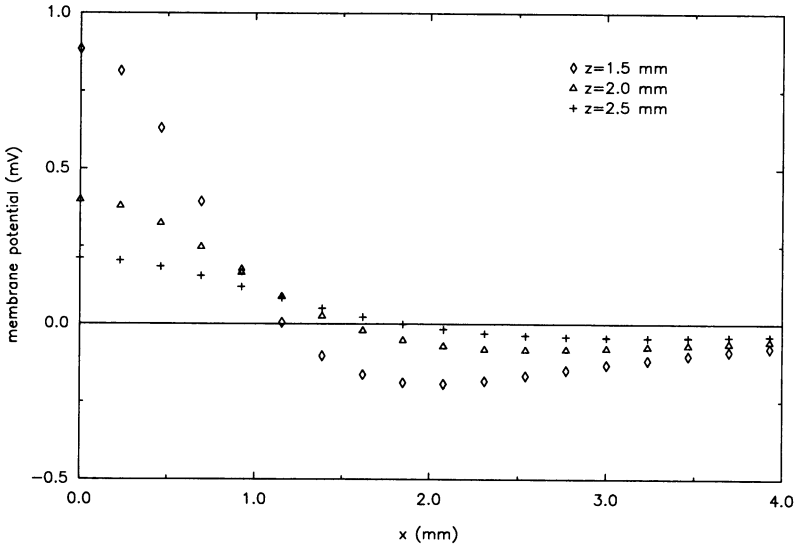

FIGURE 7 Profiles of the steady-state peak membrane potential for a 1-mA DC step positioned at $z = 1.5$ mm, $z = 2$ mm, and $z = 2.5$ mm. Results valid only at nodes of Ranvier.

tional to both the current applied and to the resistivity of the medium separating electrode and myelinated fiber. Likewise, the response is inversely proportional to the cube of the distance separating electrode and fiber. A dimensional analysis of threshold awaits further discussion of the attenuation constant Q, but it should be clear now that these relations must also hold for a nonlinear fiber model up to threshold if the excitable membrane properties are not varied between fibers. The threshold current for initiation of an action potential in a distant fiber should be proportional to the cube of the distance between the fiber and a monopolar electrode and inversely proportional to the resistivity of the medium separating them.

Distance curves

Using Eq. 6 it is possible to determine the relative response of the nearest node as the perpendicular distance of the node to the source is varied. As noted above, this should approach an inverse cubic relationship as the distance becomes large. Fig. 8 shows the relative fiber response as a function of distance at two frequencies, determined from Eq. 6. It shows that as stimulation frequency is increased, so is spatial selectivity. If an array of fibers is located at a variety of distances from a source, a high frequency stimulus will better select for the near fibers than will one at a low frequency. This property of stimulus frequency is the same as that previously described for unmyelinated fibers using a spatial frequency analysis (41). Although the linear theory is sufficient to describe the existence of this phenomenon, a quantitative analysis requires a nonlinear model because sodium channel activation is a frequency-dependent process.

Electrical tuning curves

The same calculations used in Fig. 8 can be used to plot the relative response of the nearest node as a function of frequency. This is shown in Fig. 9 which plots the electrical tuning curve of the nearest node for a variety of source distances. It is clear that the shape of the tuning curve, described by its time constant, is a function of distance from the stimulating electrode. The time constant increases with increasing distance of the source, up to $\sim z = 3$ mm, and remains constant with further distance increases. This maximal time constant is a fundamental property of the membrane and as will be demonstrated below, approximates a weighted average of the nodal and internodal time constants.

Closer look at Q and dimensional analysis

It has previously been stated, without proof, that Q as determined by Eq. 11 is a weighted average of Q_1 and Q_2. The subscript 1 refers to the node and 2 to the internode. Given

$$Q_i = \frac{1}{\lambda_i}\sqrt{1 + j\omega\tau_i},$$

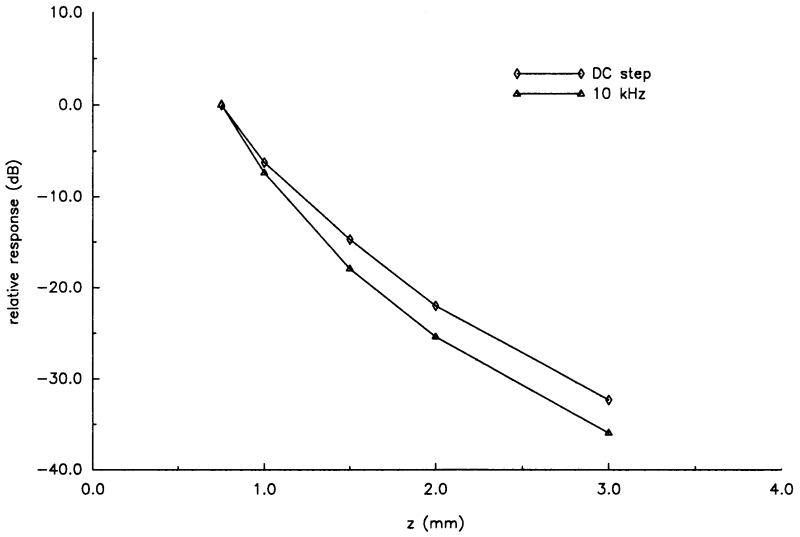

FIGURE 8 Relative magnitude of the membrane potential (fiber response) at nearest node as a function of electrode distance for DC step and 10 kHz stimuli. Responses are normalized to those at 0.75 mm.

where λ_i and τ_i are the length and time constants of the section under consideration, consider a node–internode unit for the DC case when $\omega = 0$. Under these circumstances $Q_i = 1/\lambda_i$. Assume that Q can be similarly represented by

$$Q = \frac{1}{\lambda}\sqrt{1 + j\omega\tau}. \tag{15}$$

For the DC case then $Q = 1/\lambda$. Because $\lambda = \sqrt{r_m/r_a}$, it is straightforward to apply the usual rules for lumping the parallel membrane resistances of the node and internode to show that

$$\frac{1}{\lambda^2} = \frac{1}{2l_1 + l_2}\left(\frac{2l_1}{\lambda_1^2} + \frac{l_2}{\lambda_2^2}\right). \tag{16}$$

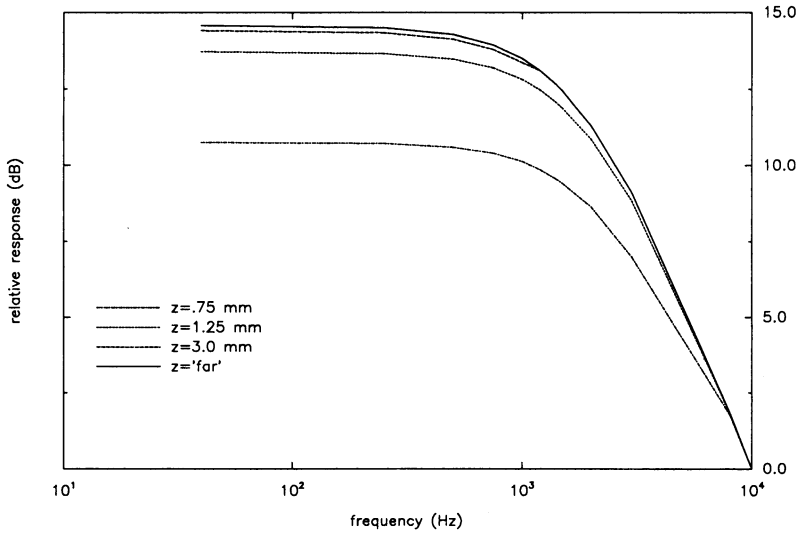

FIGURE 9 Relative tuning curves for sources positioned at $z = 0.75$ mm, $z = 1.25$ mm, $z = 3$ mm, and "far." Fiber responses are normalized to the 10 kHz response. The "far" curve is calculated from Eq. 14.

Thus λ, the length constant of the lumped node-internode, is the weighted average of λ for the node and for the internode. The lengths of the segments form the weights. A similar approach can be taken with the membrane capacitance and time constant to yield an equation for the overall time constant of the node-internode unit

$$\tau = \frac{2l_1\lambda_2^2\tau_1 + l_2\lambda_1^2\tau_2}{2l_1\lambda_2^2 + l_2\lambda_1^2}. \tag{17}$$

The time constant τ is then also a weighted average of the nodal and internodal time constants. It is the maximal time constant shown in Fig. 9.

Fig. 10 shows Q as a function of frequency calculated both from Eq. 11 and from Eq. 15, where λ and τ are obtained from Eqs. 16 and 17, respectively. The closely overlapped curves indicate that at least for this range of frequencies, Q can be represented by Eq. 15. Under these conditions, the membrane potential of the nearest node, Eq. 14, becomes

$$\overline{V}_m(z, \omega) = \frac{-\rho I\lambda^2}{4\pi z^3(1 + j\omega\tau)}. \tag{18}$$

Eq. 18, the frequency response of a simple R-C lowpass filter, can be simply transformed into the time domain and the resulting impulse response integrated to yield the step response

$$V_m(z, t) = \frac{-\rho I\lambda^2}{4\pi z^3}(1 - e^{-t/\tau}). \tag{19}$$

Thus, in addition to the effects of distance and resistivity noted above, the electrical threshold for initiation of action potentials to sinusoidal or pulsatile stimuli is inversely proportional to the square of the fiber's length constant. This permits a simple dimensional analysis of fiber threshold.

For an unmyelinated fiber, or for the nodal segment of a myelinated fiber, the length constant is given by

$$\lambda_1 = \sqrt{r_1/r_a} = \sqrt{\frac{R_1 d}{4R_a}}.$$

For the myelinated internodal segment

$$\lambda_2 = \sqrt{r_2/r_a} = \frac{d}{2}\sqrt{\frac{\pi r_2}{R_a}}.$$

Therefore λ, the overall length constant of the node-internode unit will have a dependence on axon diameter d, somewhere intermediate between the half and first power. This intermediacy will be determined by Eq. 16 which shows that the weights for the weighted average are decided by the relative lengths of the node and internode segments. Because the internode is far longer than the node, the linear term must predominate if internodal length is proportional to fiber diameter. This is shown in Fig. 11, demonstrating the linear relation between λ and fiber diameter. From the definition of Q, Eq. 15, it should be clear that the imaginary part of Q, the internodal delay, is inversely proportional to fiber diameter. Therefore the length constant is approxi-

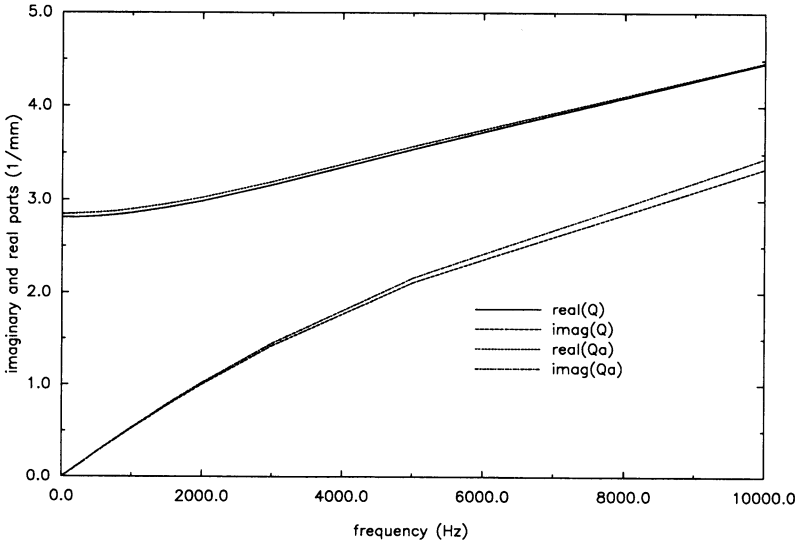

FIGURE 10 Real and imaginary parts of Q as a function of frequency. Q computed by the exact technique of Eq. 11. Qa by the weighted average technique of Eq. 15.

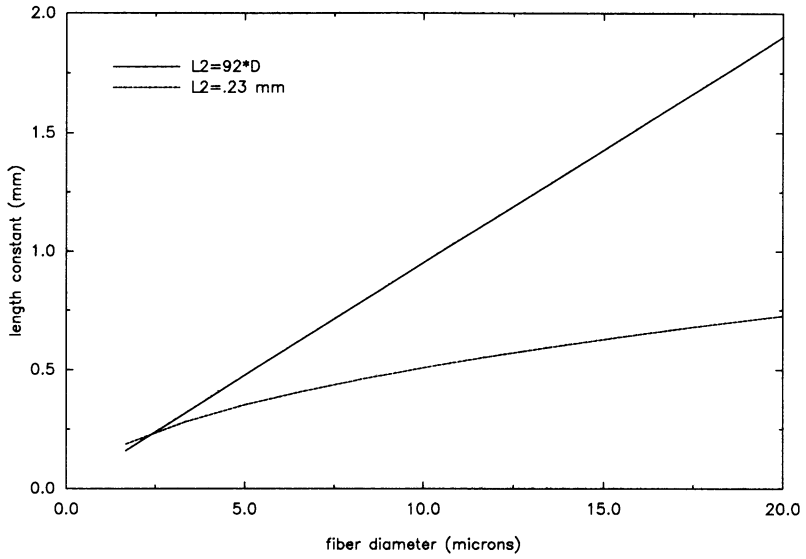

FIGURE 11 Length constant, λ, as a function of fiber diameter D as given by Eq. 16. The solid line is for internodal length proportional to fiber diameter. The interrupted line is for constant internodal length.

mately proportional to the fiber diameter for the same reasons conduction velocity is approximately proportional to fiber diameter in myelinated fibers (20, 22).

Thus, for far-field stimulation under the given assumptions, the electrical threshold for initiation of action potentials at the nearest node is inversely proportional to the square of the fiber diameter. It should therefore be possible to account for the range of far-field electrical thresholds encountered in a fiber bundle by the range of fiber diameters present in the nerve if the active fiber properties are uniform throughout this range.

Fig. 11 also shows that a nonlinear relation between length constant and fiber diameter is possible if internodal length is not linearly related to fiber diameter. While much anatomic and indirect electrophysiological data attests to the linearity of this relation (32), rigor demands direct histologic verification without possible corruption by fixation artifact.

Effects of the myelin sheath

The simplifications derived in the previous section permit a straightforward analysis of the effects of the myelin sheath on the strength-duration curve. Since the McNeal model was first developed (27), numerous nonlinear models have been described which assume the myelin to be a perfect insulator (14, 40). Following McNeal, these models assume that the myelin sheath does not significantly affect the strength-duration curve. Eq. 17 illustrates the fallacy of this assumption.

If the myelin resistance approaches an infinite value, then the internodal length constant λ_2 also approaches infinity. Under these circumstances Eq. 17 becomes

$$\tau = \tau_1.$$

The overall membrane time constant equals the specific time constant of node. Using the data set in Table 2, one can see that the nodal time constant, $\tau_1 = 34.1$ μs, is significantly less than the time constant computed using both nodal and internodal data, $\tau = 84$ μs. Bostock has shown that the nonlinear strength-duration time constant is larger than, and is a linear function of the membrane time constant (11). Therefore, a nonlinear model assuming that myelin is a perfect insulator will also underestimate the strength-duration time constant.

Models of the node–paranode region

It should be clear from the discussion of the attenuation constant Q, that changes in extracellular "polarizability" secondary to changes in passive membrane properties are entirely reflected by changes in Q. In short, the induced membrane potential at a given distance scales with Q. It is therefore possible to study different models of myelinated cables by examining the effects of changes in model parameters on Q. An important example of this was shown above in the discussion of the myelin sheath. A related question is the effect of different parameters defining the paranodal region.

The passive electrical properties of the paranodal region are uncertain at this time (12). Given this uncertainty, it is useful to examine a range of possible

models for their effects on extracellular excitability. In order of increasing complexity, it seems reasonable to consider six different node-paranode descriptions: (*a*) Classical Model: Nodal and internodal axon are the same diameter. Paranodal membrane properties are identical to internode. (*b*) Constricted Node Model: Nodal diameter is smaller than internodal diameter. Paranodal membrane properties are identical to internode. (*c*) Constricted Paranode Model: Nodal and paranodal diameters are smaller than internodal diameter. Myelin attachment segment has membrane properties identical to compact myelin. (*d*) Leaky Paranode Model: Nodal and paranodal diameters are smaller than internodal diameter. Myelin attachment segment has membrane capacitance of internode and membrane resistance of node. (*e*) Leaky Capacitive Paranode Model: Nodal and paranodal diameters are smaller than internodal diameter. Myelin attachment segment has passive membrane properties identical to node. (*f*) Tight Capacitive Paranode Model: Nodal and paranodal diameters are smaller than internodal diameter. Myelin attachment segment has membrane resistance of internode and membrane capacitance of node.

For each of these models, the overall length and time constants of the node–paranode–internode unit are summarized in Table 3. These calculations were performed assuming the node and constricted axon segment to have a diameter of $0.41d$ and a myelin attachment segment 3 μm long (9). The first three representations of the paranodal region have similar length constants and virtually identical time constants. The last three have somewhat different values although none vary by $> 24\%$. These three models are unlikely as they are inconsistent with the time constant changes that have been documented with demyelination of the paranode (12). They are included here as they represent electrically extreme cases. This illustrates that even with the most implausible paranodal models, the length and time constants are only changed by 24%.

It is noteworthy that the length constant for the first three models is approximately equal to the internodal length. While these models will conduct action potentials given sufficient peak sodium current (Rubinstein, J. T., unpublished results) they do not provide a "safety factor" for saltatory conduction. It seems reasonable to question the validity of the model parameters on this basis.

TABLE 3 Length and time constants for the six paranode models

Model	λ (*mm*)	τ (μ*s*)
a	0.24	84
b	0.24	84
c	0.23	85
d	0.20	64
e	0.20	71
f	0.23	95

TABLE 4 Sensitivity to changes in model parameters

Parameter	λ	τ
R_a	0.72–1.4	1.01–0.99
R_1	1.29–0.76	1.7–0.56
C_1	1–1	1.32–0.85
r_2	1.05–0.92	1.1–0.86
c_2	1–1	1.68–0.65

Figures are given as a–b where a represents the relative effects of doubling the parameter and b of halving it.

Sensitivity to parameter changes

In addition to varying the anatomical parameters of the model, it is of interest to vary the electrical parameters. Table 4 illustrates the effects of doubling and halving the nodal and internodal membrane parameters on the overall length and time constants. Because of the interaction between node and internode, the model is fairly robust to changes in either segment alone. It is notable that the exact myelin resistance does not appear to be of great importance despite the great relative length of the internode. This relative insensitivity to internodal parameters permits modeling electrical stimulation of mammalian nerve despite the need to use measurements of myelin resistance and capacitance from amphibian fibers.

Electrode distance: cat dorsal column

It is the author's intent to combine the myelinated fiber model described here with a volume-conduction model of the cat temporal bone (19). This combination should provide a quantitative model for electrical stimulation of the cat auditory nerve within the constraints of the experimentally measured parameters. As an independent test of the reliability of the fiber model, it is informative to compare its predictions with quantitative physiologic data from the literature. The ideal experimental preparation would consist of an isolated myelinated fiber of great length, with well-characterized membrane properties, placed in a homogeneous, isotropic medium of known resistivity, in the vicinity of a small monopolar electrode. While this ideal quantitative experiment has not been performed, a useful approximation is given by the work of BeMent and Ranck in the dorsal columns of

the cat spinal cord (38, 7, 8). Dorsal column fibers were electrically stimulated with 50 μs cathodal current pulses from macroelectrodes placed on the pial surface. The resistivity of the medium was characterized by potential measurements at varying distances from the stimulus (38). Microelectrode penetrations of known depth isolated single-unit activity. The conduction velocity, electrical threshold, strength-duration time constant, and ratio of cathodal to anodal threshold were obtained. The assumption that dorsal column fibers maintain a fairly constant position relative to the pial surface permitted the construction of threshold-distance curves for units of known conduction velocity (7).

Fig. 12 illustrates the experimental threshold-distance curves for the slowest and fastest fibers for which data are presented in reference 7. These points are plotted with the model results. Threshold is assumed to be 15 mV (8) and the scale factors relating conduction velocity and fiber diameter are 6 and 5 for the faster and slower fibers, respectively (32). Stimulation frequency is chosen to be 3.775 kHz. For an RC circuit with a time constant of 84 μs, this frequency gives a steady-state response equal to the transient response to the above experimental stimulus.

While it is not difficult to incorporate the anisotropic resistivity of the dorsal columns into the model, this was not done. There is sufficient uncertainty in the resistivity measurements (3, 37) that a homogeneous medium was assumed. The resistivity of the medium, 380 Ωcm, was chosen to provide a best fit between model and data. Note that this resistivity is well within the limits of the measured anisotropic resistivities, 138 and 1,211 Ωcm (38).

Anodal/cathodal threshold ratio

Examination of Figs. 6 and 7 should indicate that at some distance from the closest node, the membrane is polarized with opposite polarity from the closest node. Thus, if the closest node is depolarized, this "secondary site" is hyperpolarized. Anodal stimuli should depolarize this site. Due to the relative amplitude of polarization at the two sites, the model suggests that the closest node is 4.94 times more excitable than the "second site" for far-field stimuli. This far-field ratio may also be obtained from the "activating function" (39). The near-field ratio has a complex dependence on electrode-fiber distance that has not yet been completely analyzed. A sampling of 33 dorsal column fibers by BeMent and Ranck yielded an anodal/cathodal threshold ratio of 4.57 ± 1.0 (7). The conduction velocity and distance of these fibers were not specified.

DISCUSSION

A mathematical model for electrotonus in myelinated fibers has been developed and applied to the problem of extracellular electrical stimulation of nerve. It permits

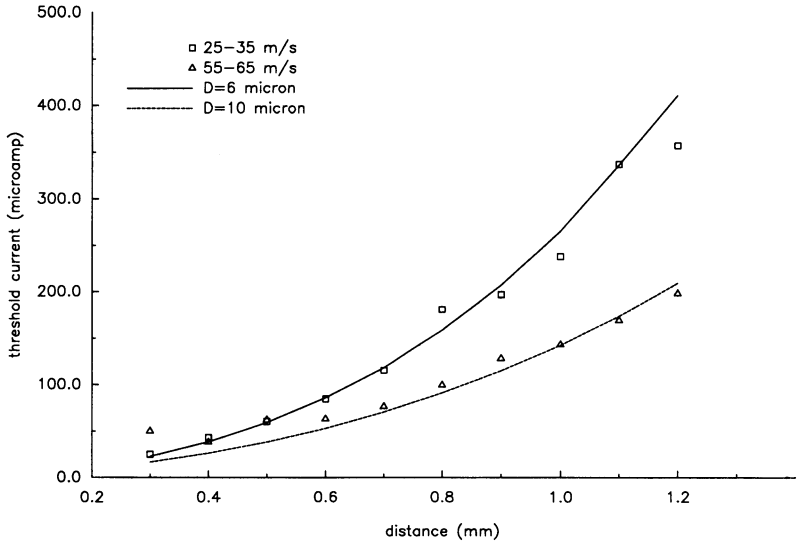

FIGURE 12 Model and experimental threshold-distance curves. Solid and dotted lines give model results for a homogeneous, isotropic medium with a resistivity of 3,800 Ωmm. Separate points are experimental results from Table 1 of reference 7. Model and experiment have correlation coefficient of 0.985.

simple calculation of the length and time constants for a fiber using weighted averages of these constants for each of the axon segments incorporated in the model. There are no theoretical restrictions on the number of axon segments in the model, so any degree of paranodal complexity may be incorporated as more data on the structure and electrical properties of the paranodal region become available. In its present form the model cannot account for possible current paths underneath the myelin sheath (6). Modeling such current paths results in a fourth order differential equation which may prove analytically tractable despite its complexity.

The linear model of myelinated fiber described here is not an attempt to replace numerical simulations of the Frankenhauser-Huxley type (20). Instead it provides a distinct complement to the nonlinear models by permitting simple calculation of the effects of model parameters on the length and time constants of the fiber. This permits the rejection of clearly implausible models before the development of a complex numerical simulation. By providing a benchmark against which linearized computer simulations may be tested, and permitting a "preview" of the small-signal membrane response, an appropriate fiber length and number of nodes may be chosen. Thus, this analytical model constitutes an important adjunct to nonlinear numerical efforts.

When the model is applied to extracellular stimulation, it permits quantitative insight into problems of both clinical and basic significance. By dimensional arguments, the model makes the following predictions for threshold to far-field, monopolar electrical stimuli: (*a*) threshold is inversely proportional to the resistivity of the medium separating electrode and fiber. (*b*) Threshold is proportional to the cube of the distance from fiber to electrode. (*c*) Threshold is inversely proportional to the square of the fiber diameter. (*d*) Threshold for monophasic anodal stimuli is 4.94 times threshold for monophasic cathodal stimuli.

For closer monopolar stimuli, the membrane time constant and the nonlinear strength-duration time constant are predicted to be a function of the electrode distance. For near sources, the time constant is less than for those more distant. Near-field stimuli are also affected by the stopbands in the spatial frequency domain that are described in the appendix. If two adjacent nodes are subjected to a similar applied field, the membrane response is poor, even if a substantial gradient is imposed along the internode. At higher temporal frequencies this effect probably becomes less important. All of these predictions require direct experimental verification.

The main limitations of any model are imposed by its assumptions. The limitation of the linearity assumption is less significant than it may seem, as the quantitative consequences of membrane nonlinearities have been well documented (11, 29). Furthermore, dimensional analysis and calculation of relative thresholds is accurate as long as stimulation frequency and sodium channel density are unchanged. Although there is evidence that small fibers are not "dimensionally similar" to large fibers (31), it seems likely that dimensional similarity is a reasonable assumption for a small range of fiber diameters.

A linear relationship between fiber diameter and internodal length is supported by numerous anatomical and indirect physiological studies (32). Because this relationship is a critical parameter for extracellular stimulation, it should be histologically verified in unfixed material.

The passive electrical properties of mammalian internodes have not been determined experimentally and represent major unknowns in any model of mammalian myelinated fibers. It should be noted however, that the model length and time constants are relatively insensitive to the internodal capacitance and remarkably unaffected by changes in the internodal resistance. Thus, activation of internodal potassium channels (10) must cause very large changes in conductance to alter substantially the results reported here.

The effects of fiber bundling are difficult to assess. Longitudinal current flow through nerve may occur in both intracellular and interstitial compartments (37). While bidomain models have been developed to analyze this complication (2, 36), they currently apply only to the steady-state stimulation of uniformly sized fiber bundles. Their application requires detailed histologic analysis of fiber packing and appropriate anisotropic nerve resistivities (3, 37). These are formidable experimental and theoretical challenges which need solution.

Threshold to extracellular stimulation, as recorded by a microelectrode at some distance from the site of activation, is a complex process. Multiple nodes can be near threshold at the same time resulting in a high degree of interaction between the spike initiation and conduction processes. Anodal block, a suprathreshold phenomenon (40), is but one example of possible field-neuron interactions that can preclude conduction of an initiated action potential. In nonlinear models, small changes in parameters, such as the maximal sodium current, can determine whether a spike initiated is conducted to the recording site (Rubinstein, J. T., unpublished results). Sophisticated nonlinear models from mammalian voltage-clamp data and significant experimental effort are needed if this process is to be understood quantitatively. The linear model provides a small, if fundamental, part of this endeavor.

EXACT SOLUTION FOR PERIODIC CABLE

Greens function

Let the point $x = 0$ be located at the center of a node. Let V_0 and I_0 be the internal voltage and longitudinal current at that site. Z is the complex impedance there. Let V_1, I_1, and V_2, I_2 be the voltage and current at the beginning of the internode and subsequent node, respectively. The regions are labeled as in Fig. 2. Let x' be the position of the extracellular voltage impulse and for the moment assume $x < x'$.

In region 1, $0 \le x \le l_1$, the potential is given by

$$\overline{G}^{(1)}(x;x') = V_0 \cosh Q_1 x - I_0 \frac{r_a}{Q_1} \sinh Q_1 x. \tag{20}$$

In region 2, $l_1 \le x \le l_1 + l_2$, by

$$\overline{G}^{(2)}(x;x') = V_1 \cosh Q_2(x - l_1) - I_1 \frac{r_a}{Q_2} \sinh Q_2(x - l_1) \tag{21}$$

and in region 3, $l_1 + l_2 \le x \le l$,

$$\overline{G}^{(3)}(x;x') = V_2 \cosh Q_1[x - (l_1 + l_2)] - I_2 \frac{r_a}{Q_1} \sinh Q_1[x - (l_1 + l_2)]. \tag{22}$$

To determine V_0 for a given x' note that the differential equation describing the Green's function is

$$\overline{G}_{xx}(x;x') - Q^2(x)\overline{G}(x;x') = -Q^2(x)\delta(x - x')$$

and integrate from $x'-$ to $x'+$ leaving

$$\overline{G}_x|_{x'-}^{x'+} = -Q^2(x').$$

Since the current on the two sides of the source must have opposite directions and it is assumed $x < x'$,

$$\overline{G}_x(x = x') = \frac{Q^2(x')}{2}.$$

If x' is in region 1, $0 \le x' \le l_1$, then

$$V_0^{(1)}(x') = \overline{G}(0;x') = \frac{Q_1^2}{2} \frac{1}{Q_1 \sinh Q_1 x' - \frac{r_a}{Z} \cosh Q_1 x'}. \tag{23}$$

If x' is in region 2, $l_1 \le x' \le l_1 + l_2$,

$$V_1 Q_2 \sinh Q_2(x' - l_1) - I_1 r_a \cosh Q_2(x' - l_1) = \frac{Q_2^2}{2}.$$

By applying the appropriate matrix transformation on V_1 and I_1 to give functions of V_0 and I_0, it can be shown that

$$V_0^{(2)}(x') = \frac{Q_2^2}{2} \frac{1}{(A_1 - B_1/Z)Q_2 \sinh Q_2 x_1' + r_a(C_1 - A_1/Z) \cosh Q_2 x_1'}, \tag{24}$$

where $V_0 = I_0 Z$. If x' is in region 3, $l_1 + l_2 \le x' \le l$, then a similar procedure gives

$$V_0^{(3)}(x') = \frac{Q_1^2}{2} \frac{1}{(D_{12} - B_{12}/Z)Q_1 \sinh Q_1 x_2' + r_a(C_{12} - A_{12}/Z) \cosh Q_1 x_2'}, \tag{25}$$

where $x_1' = x' - l_1$ and $x_2' = x' - (l_1 + l_2)$. The transformation matrices are defined in the Nonuniform Axon section, and

$$\begin{bmatrix} A_{12} & B_{12} \\ C_{12} & D_{12} \end{bmatrix} = \begin{bmatrix} A_1 & B_1 \\ C_1 & D_1 \end{bmatrix} \begin{bmatrix} A_2 & B_2 \\ C_2 & D_2 \end{bmatrix}.$$

Hartree harmonic representation

To determine the frequency response of the cable to an applied field, it is necessary to integrate the exact Green's function over the applied field. The exact Green's function for a periodic cable, $x < x'$, is given by Eqs. 20, 21, or 22, depending on the value of x, with V_0 given by Eqs. 23, 24, or 25 depending on the value of x'. Thus the Green's function is segmentally defined. It is desirable to represent the Green's function by a continuously defined function to facilitate the needed integration. Floquet's theorem permits this representation. It also eases the determination of the spatial frequency response of the fiber because that requires taking a Fourier transform in x' of the Green's function. It should be noted that this Green's function is not shift-invariant due to its asymmetry. Changes in x have different effects than changes in x', therefore much of the symmetry of the Fourier transform is lost.

Because Floquet's theorem states that all waves in a periodic structure vary identically from one period to the next except by a complex constant, it is possible to expand the Green's function in a special Fourier series. Noting that $\overline{G}(x + l) = \overline{G}(x)e^{-Ql}$, a periodic function $P(x)$ can be created with $P(x) = \overline{G}(x)e^{Qx}$. $P(x)$ can be expanded in a Fourier series

$$P(x) = \sum_{n=-\infty}^{+\infty} A_n e^{j(2\pi/l)nx},$$

where the coefficients are given by

$$A_n = \frac{1}{l} \int_0^l P(x) e^{-j(2\pi/l)nx}\, dx.$$

Thus, the original function $\overline{G}(x')$can be expanded in a Fourier series

$$\overline{G}(x') = \sum_{n=-\infty}^{+\infty} A_n e^{j\beta_n x'}, \tag{26}$$

where the coefficients are given by

$$A_n = \frac{1}{l} \int_0^l \overline{G}(x') e^{-j\beta_n x'}\, dx \tag{27}$$

and

$$\beta_n = \frac{2\pi}{l} n + jQ.$$

Each coefficient in the series is known as the space or Hartree harmonic (48).

Let the solution be restricted to the center of the nearest node, $x =$

0, fulfilling the requirement that $x < x'$. Therefore $\overline{G}(0;x') = V_0(x')$ as given in Eqs. 23–25.

To determine the Hartree harmonics for the Green's function it is necessary to reformulate the reciprocals found in the above equations. Using the power series

$$\frac{1}{1-r} = \sum_{m=0}^{\infty} r^m \quad |r| < 1$$

it is straightforward to show that in region 1, $0 \le x' \le l_1$,

$$V_0^{(1)}(x') = \frac{Q_1^2}{Q_1 - r_a/Z} \sum_{m=0}^{\infty} \left(\frac{Q_1 + r_a/Z}{Q_1 - r_a/Z}\right)^m e^{-(2m+1)Q_1 x'}.$$

In region 2, $l_1 \le x' \le l_1 + l_2$,

$$V_0^{(2)}(x') = \frac{Q_2^2}{(Q_2 - r_a/Z)A_1 - \frac{Q_2}{Z}B_1 + r_aC_1} \cdot \sum_{m=0}^{\infty} \left[\frac{(Q_2 + r_a/Z)A_1 - \frac{Q_2}{Z}B_1 - r_aC_1}{(Q_2 - r_a/Z)A_1 - \frac{Q_2}{Z}B_1 + r_aC_1}\right]^m e^{-(2m+1)Q_2 x_1'}.$$

In region 3, $l_1 + l_2 \le x' \le l$,

$$V_0^{(3)}(x') = \frac{Q_1^2}{r_a(C_{12} - A_{12}/Z) + Q_1(D_{12} - B_{12}/Z)} \cdot \sum_{m=0}^{\infty} \left[\frac{Q_1(D_{12} - B_1/Z) - r_a(C_{12} - A_{12}/Z)}{r_a(C_{12} - A_{12}/Z) + Q_1(D_{12} - B_{12}/Z)}\right]^m e^{-(2m+1)Q_1 x_2'}.$$

To calculate the coefficients of the Hartree harmonics note that

$$A_n = \frac{1}{l}\int_0^l V_0(x')e^{-j\beta_n x'}\,dx' = \frac{1}{l}\left\{\int_0^{l_1} V_0^{(1)}e^{-j\beta_n x'}\,dx' + \int_{l_1}^{l_1+l_2} V_0^{(2)}e^{-j\beta_n x'}\,dx' + \int_{l_1+l_2}^{l} V_0^{(3)}e^{-j\beta_n x'}\,dx'\right\}.$$

Therefore $A_n = [A_n^{(1)} + A_n^{(2)} + A_n^{(3)}]/l$ where

$$A_n^{(1)} = \frac{Q_1^2}{Q_1 - r_a/Z} \sum_{m=0}^{\infty} \left(\frac{Q_1 + r_a/Z}{Q_1 - r_a/Z}\right)^m \frac{1 - e^{-[(2m+1)Q_1 + j\beta_n]l_1}}{(2m+1)Q_1 + j\beta_n}$$

$$A_n^{(2)} = \frac{Q_2^2 e^{-j\beta_n l_1}}{(Q_2 - r_a/Z)A_1 - \frac{Q_2}{Z}B_1 + r_aC_1} \cdot \sum_{m=0}^{\infty} \left[\frac{(Q_2 + r_a/Z)A_1 - \frac{Q_2}{Z}B_1 - r_aC_1}{(Q_2 - r_a/Z)A_1 - \frac{Q_2}{Z}B_1 + r_aC_1}\right]^m \frac{1 - e^{-[(2m+1)Q_2 + j\beta_n]l_2}}{(2m+1)Q_2 + j\beta_n}$$

$$A_n^{(3)} = \frac{Q_1^2 e^{-j\beta_n(l_1+l_2)}}{r_a(C_{12} - \frac{A_{12}}{Z}) + Q_1(D_{12} - \frac{B_{12}}{Z})} \cdot \sum_{m=0}^{\infty} \left[\frac{Q_1(D_{12} - \frac{B_{12}}{Z}) - r_a(C_{12} - \frac{A_{12}}{Z})}{r_a(C_{12} - \frac{A_{12}}{Z}) + Q_1(D_{12} - \frac{B_{12}}{Z})}\right]^m \frac{1 - e^{-[(2m+1)Q_1 + j\beta_n]l_1}}{(2m+1)Q_1 + j\beta_n}.$$

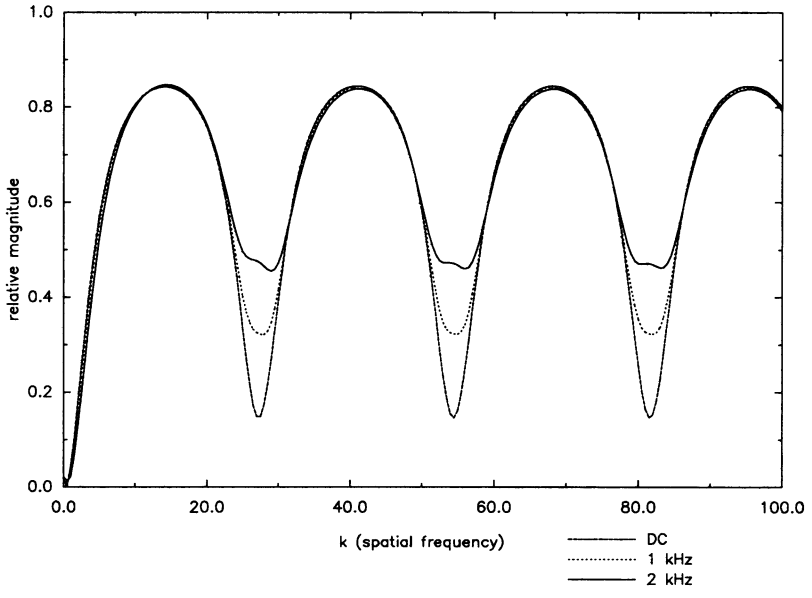

FIGURE 13 Stopbands in the spatial frequency domain. Temporal frequencies are DC, 1 kHz, and 2 kHz. Units of spatial frequency are radians per millimeter.

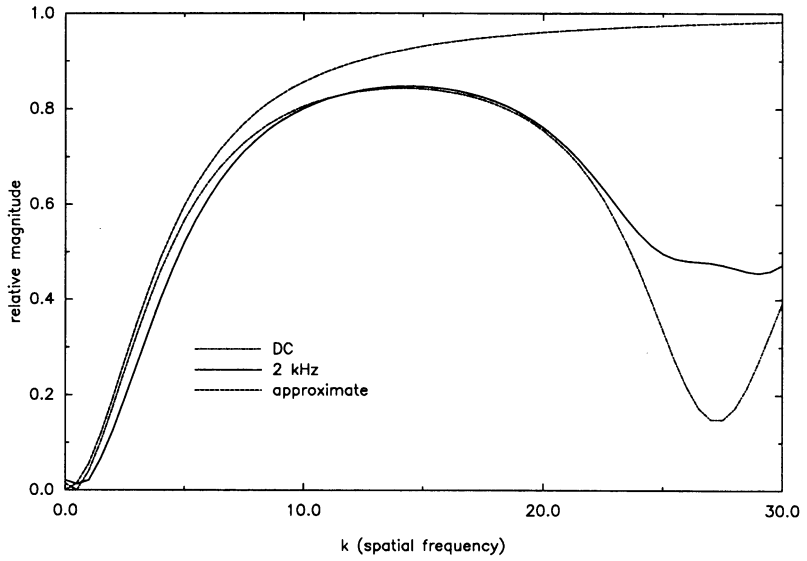

FIGURE 14 Comparison of exact DC solution and far-field approximate DC solution to spatial frequency response of nearest node. Figure also shows exact solution at 2 kHz. Units of spatial frequency are radians per millimeter.

Spatial frequency response

Consider an applied field which is symmetric about $x' = 0$. The Fourier transform of $\overline{G}(0; x')$reduces to a cosine transform. Using Eq. 26 and reversing the order of summation and integration gives

$$\overline{\overline{G}}(0; k) = 2 \sum_{n=-\infty}^{+\infty} A_n \int_0^{\infty} e^{j\beta_n x'} \cos kx' \, dx'$$

which reduces to

$$\overline{\overline{G}}(0;k) = 2j \sum_{n=-\infty}^{+\infty} A_n \frac{\beta_n}{\beta_n^2 - k^2}. \tag{28}$$

The double transform of the extracellular field $\delta(x)\delta(t)$ is unity and is subtracted from Eq. 28 with the results plotted in Fig. 13. This is the exact solution for the spatial frequency response of the nearest node at the three temporal frequencies shown. The figure shows stopbands in the spatial frequency domain occurring at integer multiples of $2\pi/l$. This occurs because when the period of a spatial frequency component is equal to l, the extracellular potential at adjacent nodes is identical. Thus, current cannot avail itself of the low-resistance pathway in and out of adjacent nodes. The inclusion of myelin conductance in the model is responsible for the stopbands being greater than zero. Indeed, at high temporal frequencies Fig. 13 demonstrates that the relative contribution of the myelin sheath to the current pathway increases significantly and reduces the depth of the stopbands.

A plot of Eq. 4, the far-field approximation for the spatial frequency response, is shown in Fig. 14 along with the exact solution. The figure illustrates that the Nyquist criterion for the far-field approximation is quite reliable as the two curves are similar up to a spatial frequency of $k = 6.8$, or one-fourth the sampling frequency. This provides a more formal proof that for far-field stimulation, the simple equations describing excitation of a continuous cable are a valid model of the electrotonic response at the midpoints of the nodes of a myelinated fiber.

The author gratefully acknowledges the thoughtful criticism of D. Eddington, N.Y.S. Kiang, J. Melcher, and the reviewers.

This work is supported by National Institutes of Health grant DC00361 and training grant DC00020.

REFERENCES

1. Abramowitz, M., and I. E. Stegun. 1972. Handbook of Functions. 10th Ed. National Bureau of Standards, Washington, D.C.
2. Altman, K. W., and R. Plonsey. 1988. Development of a model for point source electrical fibre bundle stimulation. *Med. Biol. Eng. & Comput.* 26:466–475.
3. Altman, K. W., and R. Plonsey. 1989. Analysis of the longitudinal and radial resistivity measurements of the nerve trunk. *Ann. Biomed. Eng.* 17:313–324.
4. Andrietti, F., and G. Bernardini. 1984. Segmented and "equivalent" representation of the cable equation. *Biophys. J.* 46:615–623.
5. Arnesen, A. R., and K. K. Osen. 1978. The cochlear nerve in the cat: topography, cochleotopy, and fiber spectrum. *J. Comp. Neur.* 178:661–678.
6. Barrett, E. F., and J. N. Barrett. 1987. Intracellular recording from vertebrate myelinated axons: mechanism of the depolarizing afterpotential. *J. Physiol.* 323:117–144.
7. BeMent, S. L., and J. B. Ranck. 1969. A quantitative study of electrical stimulation of central myelinated fibers. *Exp. Neurol.* 24:147–170.
8. BeMent, S. L., and J. B. Ranck. 1969. A model for electrical stimulation of central myelinated fibers with monopolar electrodes. *Exp. Neurol.* 24:171–186.
9. Berthold, C. H. 1978. Morphology of normal peripheral axons. *In* Physiology and Pathobiology of Azons. S. G. Waxman editor. Raven Press, New York. 3–63.

10. Black, J. A., J. D. Kocsis, and S. G. Waxman. 1990. Ion channel organization of the myelinated fiber. *TINS* (*Trends Neurosci.*). 13(2):48–54.
11. Bostock, H. 1983. The strength-duration relationship for excitation of myelinated nerve: computed dependence on membrane parameters. *J. Physiol.* 341:59–74.
12. Brismar, T. 1981. Electrical properties of isolated demyelinated rat nerve fibers. *Acta Physiol. Scand.* 113:161–166.
13. Brismar, T. 1980. Potential clamp analysis of membrane currents in rat myelinated nerve fibers. *J. Physiol.* 298:171–184.
14. Colombo, J., and C. W. Parkins. 1987. A model of electrical excitation of the mammalian auditory-nerve neuron. *Hear. Res.* 31:287–312.
15. Dun, F. T. 1970. The Length and Diameter of the Node of Ranvier. *IEEE* (*Inst. Electr. Electron Eng.*) *Trans. Biomed. Eng.* 17(1):21–24. 1990.
16. Finley, C., B. S. Wilson, and M. W. White. 1990. Models of neural responsiveness to electrical stimulation. *In* Cochlear Implants: Models of the Electrically Stimulated Ear. J. M. Miller and F. A. Spelman, editors. Springer-Verlag, New York.
17. FitzHugh, R. 1962. Computation of impulse initiation and saltatory conduction in a myelinated nerve fiber. *Biophys. J.* 2:11–21.
18. FitzHugh, R. 1973. Dimensional analysis of nerve models. *J. Theor. Biol.* 40:517–541.
19. Girzon, G. 1987. Investigation of current flow in the inner ear during electrical stimulation of intracochlear electrodes. M.S. thesis. Massachusetts Institute of Technology, Cambridge.
20. Goldman, L., and J. S. Albus. 1968. Computation of impulse conduction in myelinated fibers; theoretical basis of the velocity-diameter relation. *Biophys. J.* 8:596–607.
21. Gradshteyn, I. S., and J. M. Ryzhik. 1980. Table of Integrals, Series, and Products. Academic Press, Orlando, FL.
22. Jack, J. J. B., D. Noble, and R. W. Tsien. 1983. Electrical Current Flow in Excitable Cells. Clarendon, Oxford.
23. Koide, F. T. 1975. Electronus in medullated nerve. *Math. Biosci.* 25:363–373.
24. Kompaneyets, A. S., and V. T. Gurovich. 1966. Propagation of an impulse in a nerve fibre. *Biophysics* (*Engl. Transl. Biofizika*). 11:1049–1052.
25. Liberman, M. C., and M. E. Oliver. 1984. Morphometry of intracellularly labeled neurons of the auditory nerve: correlations with functional properties. *J. Comp. Neurol.* 223:163–176.
26. Markin, V. S., and Y. A. Chizmadzhev. 1967. Spread of excitation in a model of the nerve fibre. *Biophysics* (*Engl. Transl. Biofizika*). 12:1032–1040.
27. McNeal, D. R. 1976. Analysis of a model for excitation of myelinated nerve. *IEEE* (*Inst. Electr. Electron. Eng.*) *Trans. Biomed. Eng.* BME 23(4):329–337.
28. Neumcke, B., and R. Stampfli. 1982. Sodium currents and sodium-current fluctuations in rat myelinated nerve fibers. *J. Physiol.* 329:163–184.
29. Noble, D., and R. B. Stein. 1966. The threshold conditions for initiation of action potentials by excitable cells. *J. Physiol.* 187:129–162.
30. Offner, F., A. Weinberg, and G. Young. 1940. Nerve conduction theory: some mathematical consequences of Bernstein's model. *Bull. Math. Biophys.* 2:89–103.
31. Paintal, A. S. 1966. The influence of diameter of medullated nerve fibers of cats on the rising and falling phases of the spike and its recovery. *J. Physiol.* 184:791–811.
32. Paintal, A. S. 1978. Conduction properties of normal peripheral mammalian axons. *In* Physiology and Pathobiology of Axons. S. G. Waxman, editor. Raven Press, New York. 131–144.
33. Parkins, C. W., and J. Colombo. 1987. Auditory-nerve single-neuron thresholds to electrical stimulation from scala tympani electrodes. *Hear. Res.* 31:267–286.
34. Pickard, W. F. 1966. On the propagation of the nervous impulse down medullated and unmedullated fibers. *J. Theor. Biol.* 11:30–45.
35. Pickard, W. F. 1969. Estimating the velocity of propagation along myelinated and unmyelinated fibers. *Math. Biosci.* 5:305–319.
36. Plonsey, R., and K. W. Altman. 1988. Electrical stimulation of excitable cells—a model approach. *Proc. IEEE.* 76(9):1122–1129.
37. Plonsey, R., and R. C. Barr. 1986. A critique of impedance measurements in cardiac tissue. *Ann. Biomed. Eng.* 14:307–322.
38. Ranck, J. B., and S. L. BeMent. 1965. The specific impedance of the dorsal columns of cat: an anisotropic medium. *Exp. Neurol.* 11:451–463.
39. Rattay, F. 1989. Analysis of models for extracellular fiber stimulation. *IEEE* (*Inst. Electr. Electron. Eng.*) *Trans. Biomed. Eng.* 36(7):676–682.
40. Reilly, J. P., V.T. Freeman, and W. D. Larkin. 1985. Sensory effects of transient electrical stimulation—evaluation with a neuroelectric model. *IEEE* (*Inst. Electr. Electron. Eng.*) *Trans. Biomed. Eng.* 32(12):1001–1011.
41. Rubinstein, J. T., and F. A. Spelman. 1988. Analytical theory for extracellular electrical stimulation of nerve with focal electrodes I. Passive unmyelinated axon. *Biophys. J.* 54:975–981.
42. Rubinstein, J. T. 1988. Quasi-static analytical models for electrical stimulation of the auditory nervous system. Ph.D. thesis. University of Washington, Seattle.
43. Scott, A. C. 1964. Analysis of a myelinated nerve model. *Bull. Math. Biophys.* 26:247–254.
44. Scott, A. C. 1964. More on myelinated nerve model analysis. *Bull. Math. Biophys.* 29:363–371.
45. Tasaki, I. 1955. New measurements of the capacity and the resistance of the myelin sheath and the nodal membrane of the isolated frog nerve fiber. *Am. J. Physiol.* 181:639–650.
46. Veltink, P. H., J. A. van Alste, and H. B. K. Boom. 1988. Stimulation of Intrafasicular and Extraneural Nerve Stimulation. *IEEE* (*Inst. Electr. Electron. Eng.*) *Trans. Biomed. Eng.* 35(1):69–75.
47. Yeh, P., A. Yariv, and C. S. Hong. 1977. Electromagnetic propagation in periodic stratified media. I. General theory. *J. Opt. Soc. Am.* 67(4):423–438.